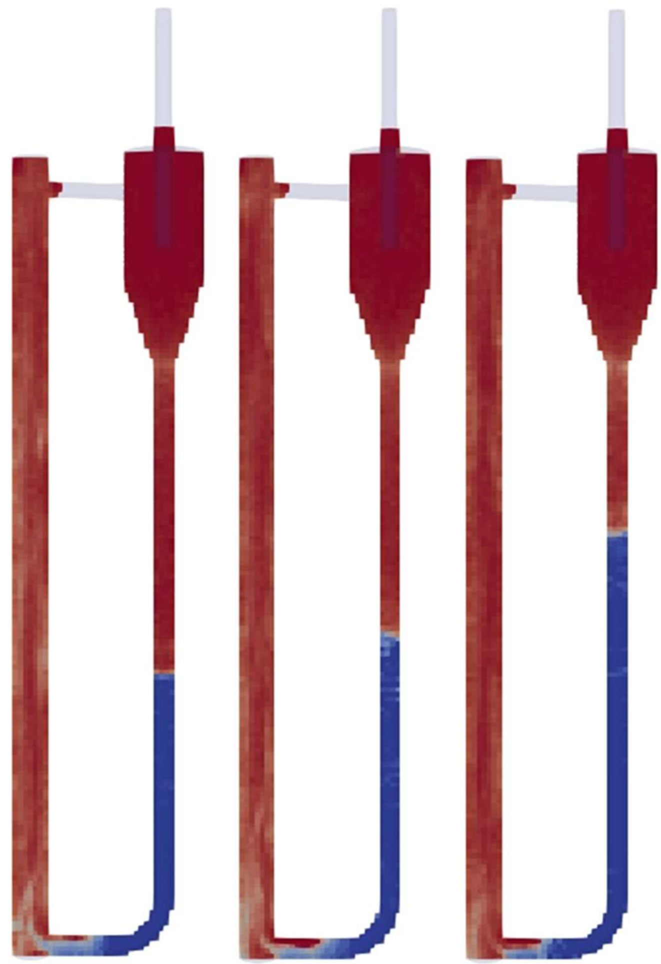

Verification and Validation of MFiX-PIC

23 January 2020

Office of Fossil Energy

NETL-TRS-2-2020

Disclaimer

Cover Illustration: Instantaneous gas volume fraction field (cross-sectional view) in a circulating fluidized bed under three different operating conditions, where the standpipe inventory changes.

Suggested Citation: Vaidheeswaran, A.; Musser, J.; Clarke, M. A. *Verification and Validation of MFiX-PIC*; NETL-TRS-2-2020; NETL Technical Report Series; U.S. Department of Energy, National Energy Technology Laboratory: Morgantown, WV, 2020; p. 48. DOI: 10.2172/1618293.

An electronic version of this report can be found at: https://netl.doe.gov/TRS

Verification and Validation of MFiX-PIC

Avinash Vaidheeswaran[1], Jordan Musser[2], Mary Ann Clarke[3]

[1]U.S. Department of Energy, National Energy Technology Laboratory, Leidos Research Support Team, 3610 Collins Ferry Road, Morgantown, WV 26507

[2]U.S. Department of Energy, National Energy Technology Laboratory, 3610 Collins Ferry Road, Morgantown, WV 26507

[3]U.S. Department of Energy, National Energy Technology Laboratory, West Virginia University Research Corporation, 3610 Collins Ferry Road, Morgantown, WV 26507

NETL-TRS-2-2020

23 January 2020

NETL Contacts:

William A. Rogers, Principal Investigator

Jonathan Lekse, Technical Portfolio Lead

Bryan Morreale, Executive Director, Research & Innovation Center

This page intentionally left blank.

Table of Contents

This page intentionally left blank.

List of Figures

List of Tables

This page intentionally left blank.

Acronyms, Abbreviations, and Symbols

Term	Description
CFD	Computational fluid dynamics
DEM	Discrete element modeling
HDPE	High-density polyethylene
MFiX	Multiphase Flow with Interphase eXchanges
MPPC	Multi-phase particle-in-cell
NETL	National Energy Technology Laboratory
ODE	Ordinary differential equation
PIC	Particle-in-cell
SS	Steady-state
SLPM	Standard Liter per minute
TFM	Two-fluid model
V&V	Verification and validation

Acknowledgments

This work was performed in support of the U.S. Department of Energy's (DOE) Fossil Energy Crosscutting Technology Research Program. The research was executed through the National Energy Technology Laboratory's (NETL) Research and Innovation Center's Advanced Reaction Systems Field Work Proposal. Research performed by Leidos Research Support Team staff was conducted under the RSS contract 89243318CFE000003.

The authors would like to thank William A. Rogers for making the data accessible for minimum fluidization test and Yupeng Xu for providing the data associated with the small-scale circulating fluidized bed used for validation in this work.

EXECUTIVE SUMMARY

This work is aimed at verification and validation (V&V) of particle-in-cell (PIC) approach in the National Energy Technology Laboratory's (NETL) Multiphase Flow with Interphase eXchanges (MFiX-PIC) which was officially released in April 2019. Under verification, the results from MFiX-PIC are compared with exact or analytical solutions, while experimental results are used for benchmarking under validation. The test suite consists of the following cases:

- Terminal velocity
- Particle advection in time-varying flow field
- Particle settling in a dense medium
- Evaporation
- Rayleigh-Taylor instability
- Minimum fluidization
- Mini-circulating fluidized bed

The cases reported in a format consistent with the existing Verification and Validation Manual (Musser et al., 2018) explore a wide range of flow velocities and concentration regimes. Only one case considered in this work verifies the implementation of heat and mass transfer routines in MFiX-PIC, while a few other studies are currently underway to further expand the validation space in reacting flows. This study highlights the need for a rigorous analysis to objectively quantify the effect of model parameters. In addition, there is a scarcity of high-quality experimental data in the literature suitable for validating PIC methodology. Future efforts would include performing experiments which provide results for a valuable database. While designing such experiments, particle count should be significant to have sufficient particles per parcel while maintaining an optimal parcel to cell volume ratio. Also, datasets should have objectively assessed experimental uncertainty whereby confidence interval in those measurements become more explicit.

1. INTRODUCTION

Particle-In-Cell (PIC) approach has gained considerable attention in industrial applications having gas-solid multi-component flows. The methodology was initially proposed by Andrews and O'Rourke (1996) for one-dimensional systems and later extended to three-dimensional systems by Snider (2001). While CPFD Software, LLC develops and maintains the original multi-phase PIC (MPPIC) model of Snider and his co-workers (Snider, 2001; O'Rourke et al., 2009; O'Rourke and Snider, 2012, 2014), open-source options are available in Multiphase Flow with Interphase eXchanges (MFiX)-PIC and OpenFOAM. In the PIC process the gas-phase is treated using an Eulerian framework while particles are grouped into computational parcels and tracked as discrete entities. The collisions between particles within parcels are not resolved, but modeled using an inter-particle collisional stress term. The stress expression is derived from Auzerias et al. (1988). In addition, there are various numerical parameters used in conditional statements inside PIC routines, and their influence on the results is not yet quantified. Despite these shortcomings, PIC methodology has been proven to model gas-solid systems reasonably well. While not being as accurate as discrete element modeling (DEM) approach, considerable speed-up is achievable using MFiX-PIC for large-scale systems.

Verification and validation (V&V) is a critical component when developing a numerical methodology such as PIC. While verification is used to establish if the discretized equations are being solved correctly, validation determines if the right equations and constitutive relations are being used to model the physical system. V&V in effect establishes the predictive capability of numerical techniques. Multiple organizations including NASA (Steele, 2016), AIAA (1998), ASME (Committee, 2009), and the U.S. Department of Defense (Allen, 2009) have developed frameworks for following V&V procedures. Recently Gel at al. (2018) proposed an extended workflow for V&V applied to granular and multiphase flow systems, which included more rigorous procedures including design of experiments and a simulation campaign. Over the past few years, the multiphase flow science team at the National Energy Technology Laboratory (NETL) has focused on V&V of the MFiX suite, which has resulted in a number of published research related to V&V (Bakshi et al., 2018; Gel et al., 2016, 2017, 2018; Shahnam et al., 2016) along with the documentation of V&V applied to MFiX-TFM and MFiX-DEM (Musser et al., 2018).

This report discusses results from V&V of MFiX-PIC (released in April 2019). Multiple test cases are selected covering a broad spectrum of hydrodynamics and spatio-temporal scales, which are restricted to systems with mono-dispersed particles having no more than one particle-phase. The results are presented based on optimal values of PIC parameters. The results point to the need for a rigorous analysis to characterize their sensitivities to different response quantities. Also, the grid size used in the current analysis is such that the ratio of single parcel volume to grid volume is not more than 5%. This is expected to account for a physically consistent stress field in dense regions. The remainder of the work is organized as follows. MFiX-PIC verification tests are presented in Section 2, and MFiX-PIC validation tests are presented in Section 3. Some of the conclusions drawn from our current study are presented in Section 4 along with plans for future work.

2. VERIFICATION

2.1 TERMINAL VELOCITY

Description

This case is similar to "DEM06: Single particle, terminal velocity" in the MFiX V&V Manual (Musser et al., 2018). A computational parcel containing physical particles is subjected to a uniform gas velocity. The statistical weight and initial gas volume fraction are adjusted such that all particles are accommodated in one parcel for the given grid resolution. The simulation results are compared with the analytical results obtained by solving the following system of Ordinary Differential Equations:

$$\frac{d^2y}{dt^2} = \frac{dv_p}{dt} = \frac{g\left(\rho_p - \rho_g\right)}{\rho_p} - \frac{3}{4}\frac{\rho_g\left|v_p - v_g\right|^2}{d_p\rho_p}C_d \tag{1}$$

The initial and the boundary conditions are given by,

$$y(0) = h_0;\ v_p(0) = 0 \tag{2}$$

where, y is the position of particle center measured from the bottom wall, v_p and v_g are the particle and gas velocities, ρ_p and ρ_g are particle and gas densities, d_p is the particle diameter, h_0 is the initial height of the particle, g is the acceleration due to gravity, and C_d is the drag coefficient. In this case, $C_d = 1$ is used for simplicity. The effect of the parcel on the gas phase is neglected since the particle concentration is extremely dilute. Hence, the momentum equations for the gas-phase are not solved.

Setup

Computational/Physical Model

3D, transient
Multiphase
Thermal energy equation is not solved
Turbulence equations are not solved (Laminar)
Uniform mesh
First order upwind discretization scheme

Geometry

Coordinate system	Cartesian	Grid Partitions
Channel length, L (x)	0.01 (m)	5
Channel height, H (y)	0.30 (m)	60
Channel width, W (z)	0.01 (m)	5

Material		
Gas density, ρ_g	1.2 ($kg \cdot m^{-3}$)	
Gas viscosity, μ_g	1.8E-5 (Pa·s)	
Solids Type	PIC	
Diameter	0.1 (mm)	
Density	2,000 ($kg \cdot m^{-3}$)	
Solids Properties (PIC)		
Pressure linear scale factor, P_s	100.0 ($N\ m^{-2}$)	
Exponential scale factor, γ	3.0 (-)	
Statistical weight	100 (-)	
Initial Conditions		
x-velocity, u_g	0.0 ($m \cdot s^{-1}$)	
y-velocity, v_g	0.4 ($m \cdot s^{-1}$)	
z-velocity, w_g	0.0 ($m \cdot s^{-1}$)	
Solids concentration, ε_s	0.0001 (-)	
Gas volume fraction at packing, ε_g^*	0.4 (-)	
Pressure, p_g	101,325 (Pa)	
Boundary Conditions		
South boundary	0.4 ($m \cdot s^{-1}$)	Mass inflow
North boundary	101,325 (Pa)	Pressure outflow
West, east, top and bottom boundaries		Free-slip wall

Results

As the parcel falls, its velocity increases initially, and reaches its terminal velocity when the gravitational force is balanced by the drag force. The numerical solution to the system of equations is obtained using 4th order Runge-Kutta method. The values are compared with the MFiX-PIC simulations as shown in Figure 1. The velocity and position are accurately predicted by MFiX-PIC as was the case with MFiX-DEM discussed in the MFiX V&V Manual (Musser et al., 2018).

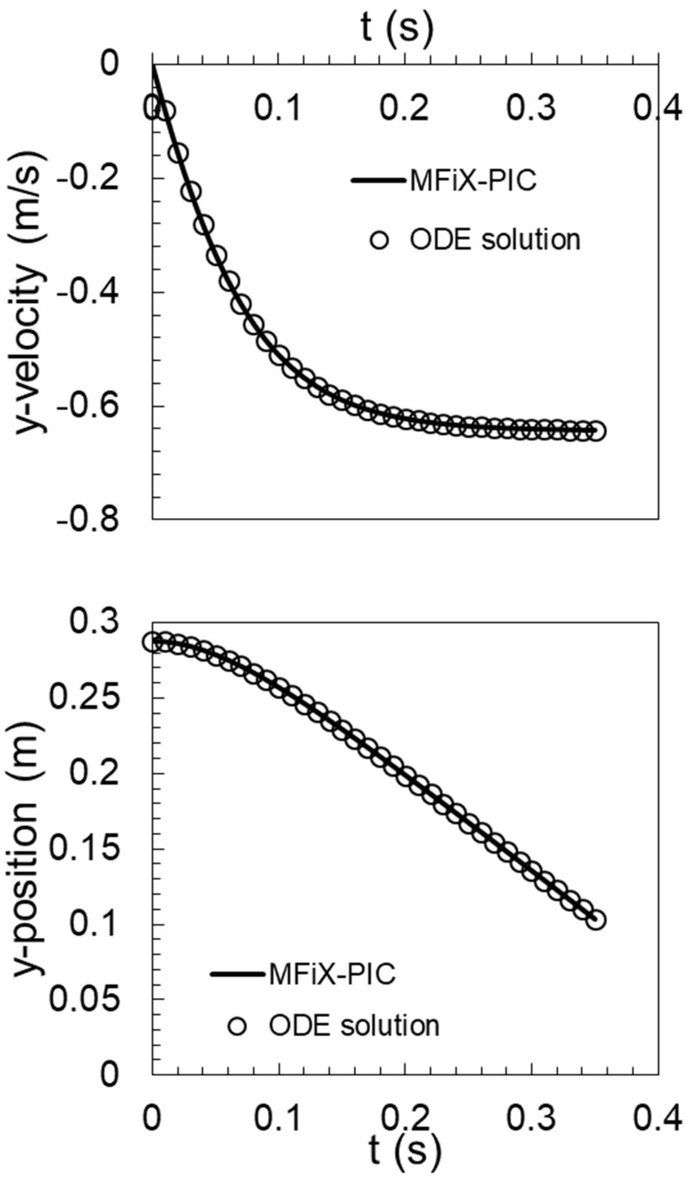

Figure 1: Predictions using MFiX-PIC: velocity (top) and position (bottom).

2.2 ADVECTION IN TIME VARYING FLOW FIELD

2.2.1 Velocity Interpolation Verification

Description

This is a code verification problem discussed in the DEM documentation of Garg et al. (2010). A total of 512 parcels are arranged on a sphere having a radius of 0.15 m centered at (0.35 m, 0.35 m, 0.35 m). The domain under consideration is a unit box (1.0 m X 1.0 m X 1.0 m) discretized uniformly having 32 cells in each direction. A time varying flow-field is prescribed as follows:

$$u_g = 2\sin^2 \pi x \sin 2\pi y \sin 2\pi z \cos\left(\frac{\pi t}{T}\right)$$

$$v_g = -\sin 2\pi x \sin^2 \pi y \sin 2\pi z \cos\left(\frac{\pi t}{T}\right) \qquad (3)$$

$$w_g = -\sin 2\pi x \sin 2\pi y \sin^2 \pi z \cos\left(\frac{\pi t}{T}\right)$$

A value of 0.25 is chosen for the time period T and the simulations are run for a total duration of 4 seconds which is equivalent to 16 cycles. The initial parcel configuration and velocities are specified through a particle_input.dat file, typical of MFiX runs that require an exact particle arrangement.

Setup

Computational/Physical Model

3D, Transient
Multiphase
Thermal energy equation is not solved
Turbulence equations are not solved (Laminar)
Uniform mesh
First order upwind discretization scheme

Geometry

Coordinate system	Cartesian	Grid Partitions
Channel length, L (x)	1.0 (m)	32
Channel height, H (y)	1.0 (m)	32
Channel width, W (z)	1.0 (m)	32

Material

Gas density, ρ_g	1.2 (kg·m^{-3})
Gas viscosity, μ_g	1.8E-5 (Pa·s)

Solids Type PIC

Diameter	0.01 (mm)
Density	2,700 ($kg \cdot m^{-3}$)

Solids Properties (PIC)

Pressure linear scale factor, P_s	100.0 ($N\ m^{-2}$)
Exponential scale factor, γ	3.0 (-)
Statistical weight	1 (-)

Initial Conditions

x-velocity, u_g	Equation (3) ($m \cdot s^{-1}$)
y-velocity, v_g	Equation (3) ($m \cdot s^{-1}$)
z-velocity, w_g	Equation (3) ($m \cdot s^{-1}$)
Gas-phase volume fraction, ε_g	1.0 (-)
Packed bed volume fraction, ε_g^*	0.4 (-)
Pressure, p_g	101,325 (Pa)

Boundary Conditions

All boundaries are cyclic

Results

The parcels are sheared in different directions since the center of the spherical arrangement is off from the center of the vortex field. Once the simulation begins, the configuration is deformed and then restored at multiples of time period T as shown in Figure 2. The absolute difference between the exact location and the numerical solution is shown in Table 1. The maximum locational error is still within 0.01 m at the end of 16 cycles.

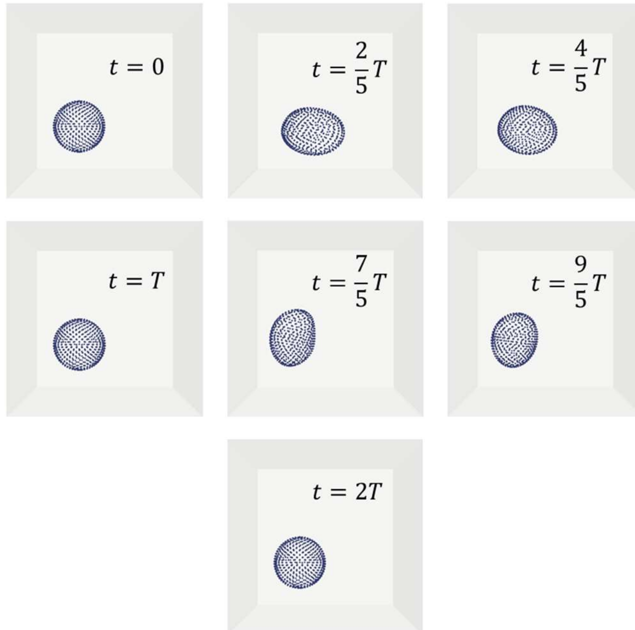

Figure 2: Instantaneous location of parcels for the configuration centered at X=0.35 m, Y=0.35 m, Z=0.35 m. The time stamps are provided inside each snapshot.

Table 1: L1-Norms of Parcel Displacement for the Configuration Centered at (0.35 m, 0.35 m, 0.35 m) having a Radius of 0.15 m

Physical Time (s)	Cycle	Maximum L1-Norm (m)
0.25	1	2.11E-03
0.50	2	1.22E-03
0.75	3	2.59E-03
1.00	4	2.44E-03
1.25	5	3.46E-03
1.50	6	3.65E-03
1.75	7	4.49E-03
2.00	8	4.87E-03
2.25	9	5.60E-03
2.50	10	6.08E-03
2.75	11	6.74E-03
3.00	12	7.29E-03
3.25	13	7.90E-03
3.50	14	8.51E-03
3.75	15	9.08E-03
4.00	16	9.72E-03

2.2.2 Parcel Volume Deposition Verification

Description

In this case the arrangement of 480 parcels having a radius of 0.15 m centered at the origin is considered. The objective is to test the following:

1. Periodic boundaries
2. Parcel volume deposition on Eulerian cells

The time varying flow-field is prescribed using Equation (3), where the time period T is 0.25 seconds. The domain under consideration and its discretization are identical to the set-up described in Section 2.2.1. The initial parcel configuration is specified through a particle_input.dat file.

Setup

Computational/Physical Model

3D, Transient
Multiphase
Thermal energy equation is not solved
Turbulence equations are not solved (Laminar)
Uniform mesh
First order upwind discretization scheme

Geometry

Coordinate system	Cartesian	Grid Partitions
Channel length, L (x)	1.0 (m)	32
Channel height, H (y)	1.0 (m)	32
Channel width, W (z)	1.0 (m)	32

Material

Gas density, ρ_g	1.2 ($kg \cdot m^{-3}$)
Gas viscosity, μ_g	1.8E-5 (Pa·s)

Solids Type	PIC
Diameter	0.01 (mm)
Density	2,700 ($kg \cdot m^{-3}$)

Solids Properties (PIC)

Pressure linear scale factor, P_s	100.0 ($N\ m^{-2}$)
Exponential scale factor, γ	3.0 (-)
Statistical weight	1 (-)

Initial Conditions

x-velocity, u_g	particle_input.dat ($m \cdot s^{-1}$)
y-velocity, v_g	particle_input.dat ($m \cdot s^{-1}$)

z-velocity, w_g	particle_input.dat ($m \cdot s^{-1}$)
Gas-phase volume fraction, ε_g	1.0 (-)
Packed bed volume fraction, ε_g^*	0.4 (-)
Pressure, p_g	101,325 (Pa)

Boundary Conditions

All boundaries are cyclic

Once the simulation begins, parcels move in all possible directions and across the periodic boundaries as shown in Figure 3. The volume conservation is examined by comparing the volume fractions of fluid and solid during the simulation as given in Table 2. The volume fraction of fluid is calculated by the code, based on interpolation of solid volumes on to the Eulerian cells and the volume fraction of solids is calculated using the particle count. It can be seen that fluid and solid volume fractions do sum to 1 (very close to machine precision). This is indicated by the negligible relative error of the sum of phasic volume fractions in Table 2. Hence, this study concluded that the implementation of routines pertaining to periodicity and parcel-fluid interpolation are verified.

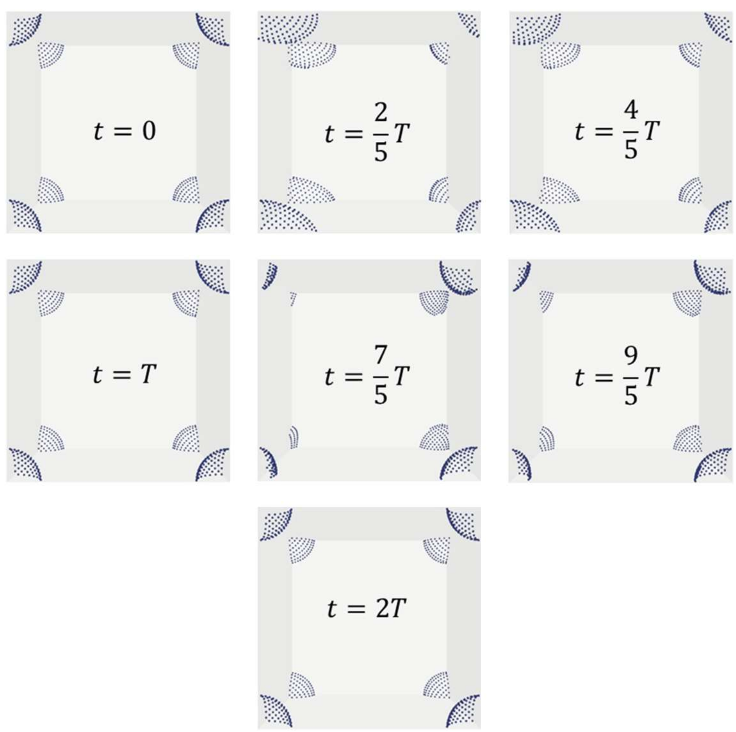

Figure 3: Instantaneous location of parcels for the configuration centered at X=0 m, Y=0 m, Z=0 m. The time stamps are provided inside each snapshot.

Table 2: Absolute Error in Total Volume Fraction for the Configuration Centered at X=0 m, Y=0 m, Z=0 m

Physical Time (s)	Cycle	Solids Volume Fraction	Gas Volume Fraction	Absolute Error
0.25	1	2.51E-04	9.997487E-01	6.66E-16
0.50	2	2.51E-04	9.997487E-01	8.88E-16
0.75	3	2.51E-04	9.997487E-01	3.33E-16
1.00	4	2.51E-04	9.997487E-01	8.88E-16
1.25	5	2.51E-04	9.997487E-01	4.44E-16
1.50	6	2.51E-04	9.997487E-01	1.33E-15
1.75	7	2.51E-04	9.997487E-01	8.88E-16
2.00	8	2.51E-04	9.997487E-01	0
2.25	9	2.51E-04	9.997487E-01	1.67E-15
2.50	10	2.51E-04	9.997487E-01	4.44E-16
2.75	11	2.51E-04	9.997487E-01	2.22E-16
3.00	12	2.51E-04	9.997487E-01	0
3.25	13	2.51E-04	9.997487E-01	4.44E-16
3.50	14	2.51E-04	9.997487E-01	1.11E-15
3.75	15	2.51E-04	9.997487E-01	1.11E-15
4.00	16	2.51E-04	9.997487E-01	6.66E-16

2.3 PARTICLE-SETTLING IN FLUID

Description

MFiX-TFM, MFiX-DEM and MFiX-PIC are used to simulate the problem of particle settling. Spatial locations of concentration fronts at time *t* = 1 seconds are compared with the analytical expression given by,

$$x(t) = x_0 + tu_{shock} \tag{4}$$

The velocity of propagation of the shock wave (derived in the Appendix) is given by,

$$u_{shock} = -\left(j + \frac{(\varepsilon_s \varepsilon_g u_r)_B - (\varepsilon_s \varepsilon_g u_r)_A}{\varepsilon_{sB} - \varepsilon_{sA}}\right) \tag{5}$$

where the subscripts A and B denote the regions on either side of the shock as shown in Figure 16. The volumetric flux is 0 in the case of settling. Also, the particle volume fraction in region A is 0 for the shock front traveling downwards. Hence the location of the shock is given by,

$$x(t) = x_0 - t(\varepsilon_{g0} u_{r0}) \tag{6}$$

where ε_{g0} is the initial gas volume fraction. The relative velocity using the Stokes drag law is given by,

$$u_{r0} = \frac{g\Delta\rho d_p^2}{18\mu_g} \varepsilon_{g0}^{3.65} \tag{7}$$

The location of the shock front corresponding to filling is given by,

$$x(t) = -t\left(\frac{\varepsilon_s^* \varepsilon_g^* u_r^* - \varepsilon_{s0} \varepsilon_{g0} u_{r0}}{\varepsilon_s^* - \varepsilon_{s0}}\right) \tag{8}$$

Setup

Computational/Physical Model

- 3D, transient
- Multiphase
- Thermal energy equation is not solved
- Turbulence equations are not solved (Laminar)
- Uniform mesh
- First order upwind discretization scheme

Geometry

Coordinate system	Cartesian	Grid Partitions
Channel length, L (x)	0.02 (m)	5
Channel height, H (y)	1.00 (m)	100
Channel width, W (z)	0.02 (m)	5

Material

Gas density, ρ_g	1,000.0 ($kg \cdot m^{-3}$)
Gas viscosity, μ_g	0.001 ($Pa \cdot s$)
Solids type	PIC,DEM,TFM
Diameter	1.0 (mm)
Density	2,000 ($kg \cdot m^{-3}$)

Solids Properties (PIC)

Pressure linear scale factor, P_s	10.0 ($N\ m^{-2}$)
Exponential scale factor, γ	3.0 (-)
Statistical weight	5 (-)
Solids slip velocity scale factor	0.5 (-)

Solids Properties (DEM)

Coefficient of friction, μ_{pp}, μ_{pw}	0.1 (-)
Coefficient of restitution, e_{pp}, e_{pw}	0.9 (-)
Spring constant, k_{pp}, k_{pw}	100.0 ($N\ m^{-1}$)

Initial Conditions

x-velocity, u_g, u_m	0.0 ($m \cdot s^{-1}$)
y-velocity, v_g, v_m	0.0 ($m \cdot s^{-1}$)
z-velocity, w_g, w_m	0.0 ($m \cdot s^{-1}$)
Location of the shock	0.8 (m)
Solids concentration, ε_{s0}	0.10, 0.15, 0.20 (-)
Gas volume fraction at packing, ε_g^*	0.6 (-)
Pressure, p_g	101,325 (Pa)

Boundary Conditions

Cyclic in x,z directions		
South boundary	0.0 ($m \cdot s^{-1}$)	Free-slip wall
North boundary	0.0 ($m \cdot s^{-1}$)	Free-slip wall

Results

The solutions from MFiX-PIC, MFiX-DEM, and MFiX-TFM are compared with the analytical expression in Figure 4. Linear-hat scheme is used to interpolate between the Eulerian and Lagrangian fields. MFiX-TFM solutions based on continuum formulation are observed to be free from oscillations in the volume fraction field for all the cases considered. Besides, the time evolution of wave fronts is also shown for simulations corresponding to ε_{s0}=0.15 in Figure 5. The results are in good agreement with the analytical solution. Further, the influence of initial solids fraction on the modelling accuracy is tested. The shock wave corresponding to filling (traveling upwards) is predicted reasonably well by all the models. This verifies the implementation of algorithms corresponding to packed regions. The analytical values along with model predictions are summarized in Table 3 and Table 4 for settling and filling wave fronts. The location of the filling wave front is determined by the occurrence of first local minima in the gradient of void fraction ε_g, while the settling wave front is determined by the last local minima in the gradient. The uncertainty values associated with the computational results correspond to cell width (0.01 m) since the shock front is estimated from discrete values.

Table 3: Location of Settling Wave Moving in the Direction of Gravity (m)

	ε_{s0} =0.10	ε_{s0} =0.15	ε_{s0} =0.20
Analytical	0.466	0.544	0.607
MFiX-PIC	0.455 ± 0.01	0.521 ± 0.01	0.583 ± 0.01
MFiX-DEM	0.455 ± 0.01	0.515 ± 0.01	0.575 ± 0.01
MFiX-TFM	0.475 ± 0.01	0.555 ± 0.01	0.615 ± 0.01

Table 4: Location of Filling Wave Moving Against the Direction of Gravity (m)

	ε_{s0} =0.10	ε_{s0} =0.15	ε_{s0} =0.20
Analytical	0.058	0.075	0.085
MFiX-PIC	0.067 ± 0.01	0.093 ± 0.01	0.107 ± 0.01
MFiX-DEM	0.069 ± 0.01	0.095 ± 0.01	0.115 ± 0.01
MFiX-TFM	0.065 ± 0.01	0.085 ± 0.01	0.095 ± 0.01

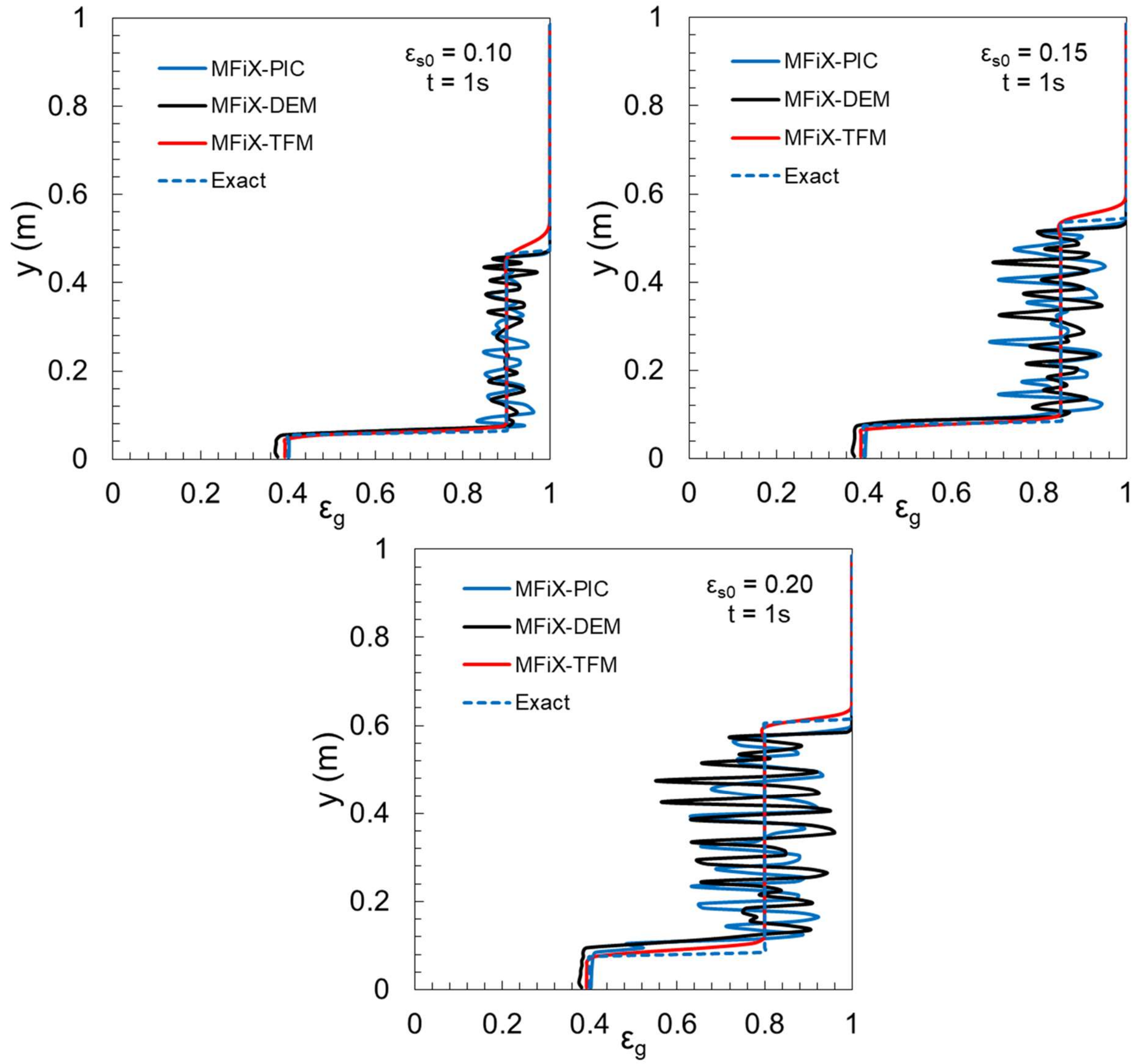

Figure 4: Solutions for different initial particle concentration ε_{s0}= (a) 0.10, (b) 0.15, (c) 0.20.

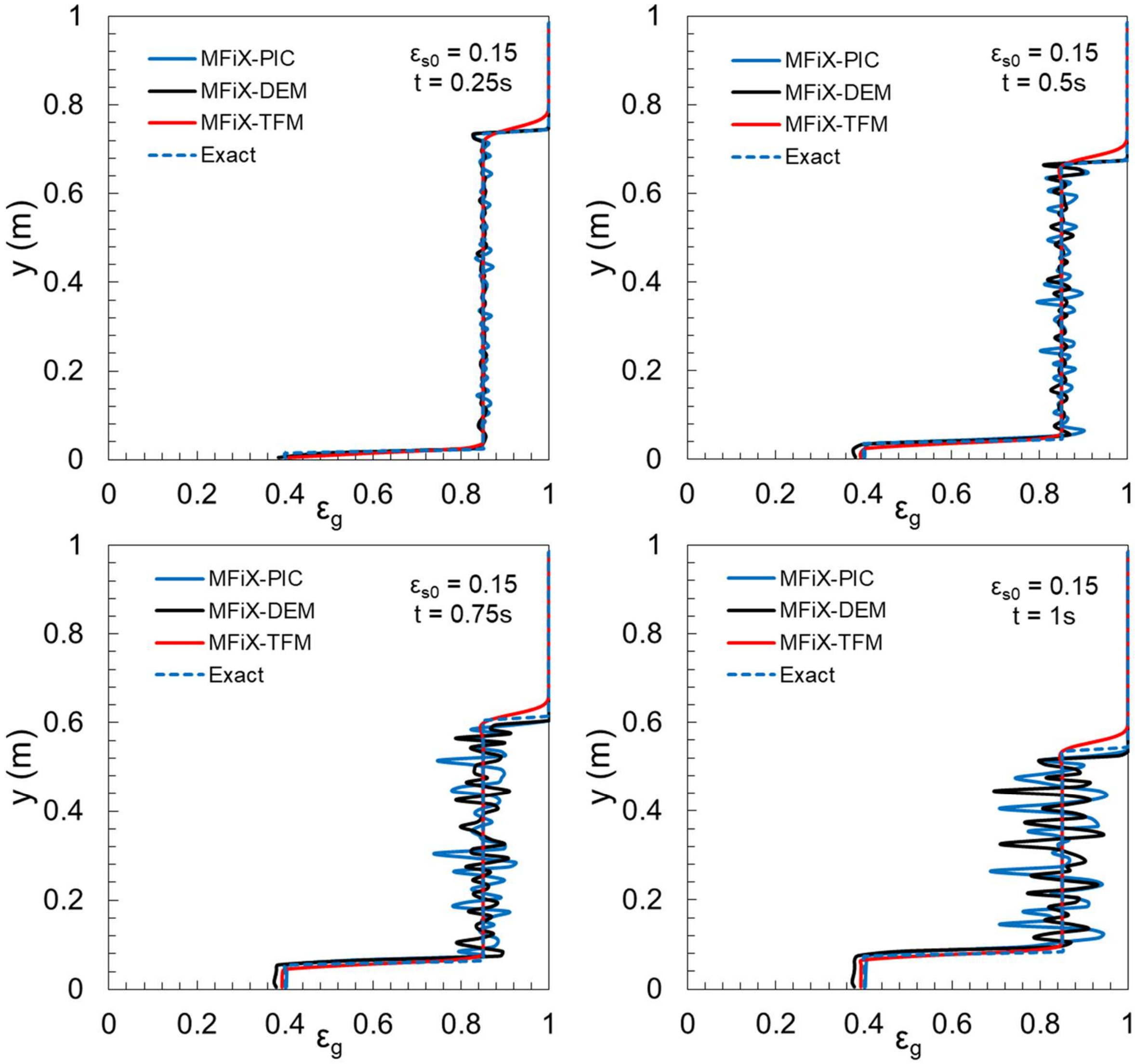

Figure 5: Time evolution of shock fronts, initial particle concentration ε_{s0}= 0.15.

2.4 EVAPORATION

Description

This case is used to verify the transport equations governing energy and species conservation. The setup consists of a single parcel representing a droplet suspended in a humidified air stream. This reflects the wet bulb phenomenon, where evaporation from the droplet results in a lowered humidified air temperature. The following reaction represents species transfer from the suspended droplet:

$$H_2O_{(l)} \rightarrow H_2O_{(g)} \tag{9}$$

Fifteen seconds of physical time is simulated to ensure the droplet achieves a steady-state (SS) temperature. The SS temperature should then compare with the theoretical wet-bulb temperature.

Setup

Computational/Physical Model

3D, transient
Multiphase
Turbulence equations are not solved (Laminar)
Uniform mesh
First order upwind discretization scheme

Geometry

Coordinate system	Cartesian	Grid Partitions
Channel length, L (x)	0.01 (m)	1
Channel height, H (y)	0.01 (m)	1
Channel width, W (z)	0.01 (m)	1

Material

Gas density, ρ_g	Calculated using ideal gas law
Gas viscosity, μ_g	0.1 (Pa·s)
Solids Type	DEM, PIC
Diameter	0.2 (mm)
Density	958.6 (kg·m^{-3})

Solids Properties (PIC)

Pressure linear scale factor, P_s	0.0 (N m^{-2})
Exponential scale factor, γ	1.0 (-)
Statistical weight	25 (-)

Solids Properties (DEM)

Coefficient of friction, μ_{pp}, μ_{pw}	0.0 (-)

Coefficient of restitution, e_{pp}, e_{pw}	1.0 (-)	
Spring constant, k_{pp}, k_{pw}	0.1 (N m^{-1})	
Initial Conditions		
x-velocity, u_g	3.0 (m·s^{-1})	
y-velocity, v_g	0.0 (m·s^{-1})	
z-velocity, w_g	0.0 (m·s^{-1})	
Gas volume fraction, ε_s	0.999894 (-)	
Solids packing fraction, ε_s^*	0.6 (-)	
Pressure, p_g	101,325 (Pa)	
Gas temperature, T_g	303.15 (K)	
Solid temperature, T_s	303.15 (K)	
Species fraction of air, X_{g1}	Varied (-)	
Species fraction of water vapor, X_{g2}	Varied (-)	
Boundary Conditions		
West boundary	Varied (kg·s^{-1}) X_{g1}, X_{g2} Varied	Mass inflow
East boundary	101,325 (Pa)	Pressure outflow
North, south, top and bottom boundaries		Free-slip wall

Results

MFiX-PIC and MFiX-DEM simulations are performed by varying the relative humidity of surrounding air. Table 5 summarizes the different settings of relative humidity and the corresponding wet bulb temperatures. Based on the comparison of the data from Mills (1999) it can be concluded that the predictions from MFiX-PIC simulations are accurate (Figure 6). Also, the results are consistent with the predictions from MFiX-DEM.

Table 5: Relative Humidity and the Corresponding Wet Bulb Temperatures

Relative Humidity (%)	Mass Fraction Air, X_{g1}	Mass Fraction Water, X_{g2}	Mass Flow Rate (g/cm)	Wet Bulb Temp (°C)
0	1.000000	0.000000	0.349315	10.5
10	0.997390	0.002610	0.348762	13.2
20	0.994771	0.005229	0.348208	15.7
30	0.992144	0.007856	0.347655	18.0
40	0.989509	0.010491	0.347102	20.1
50	0.986865	0.013135	0.346548	22.0
60	0.984212	0.015788	0.345995	23.8
70	0.981552	0.018448	0.345442	25.5
80	0.978882	0.021118	0.344888	27.1
90	0.976204	0.023796	0.344335	28.6
100	0.973518	0.026482	0.343281	30.0

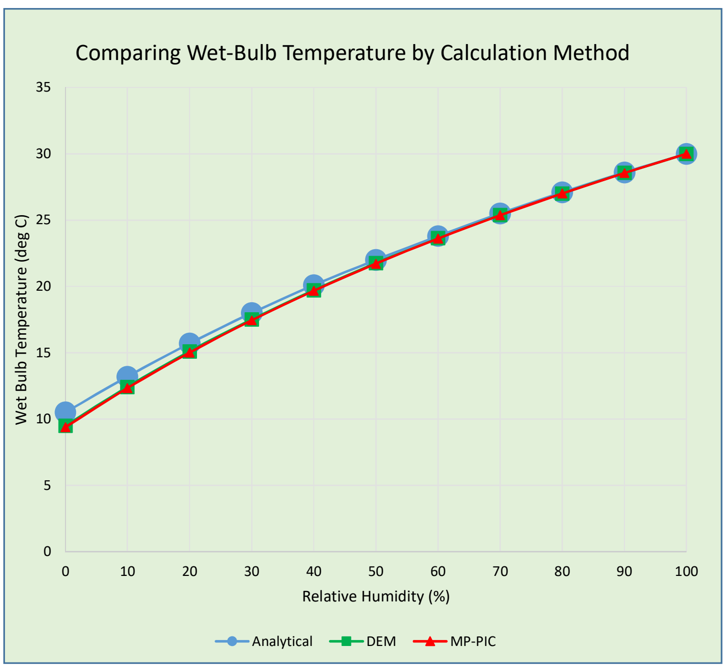

Figure 6: Comparison of wet bulb temperatures between data, MFiX-DEM and MFiX-PIC.

3. VALIDATION

3.1 RAYLEIGH-TAYLOR INSTABILITY

Description

The simulation of Rayleigh-Taylor instability using PIC methodology follows the work of Snider (2001). The domain is initialized with a lighter phase at the bottom and a heavier phase at the top. When the simulation begins, the phases invert, and the growth of a mixing layer is recorded as a function of time. Researchers in the past have proposed the following functional form for the development of the mixing layer,

$$h = \alpha A g t^2, \tag{10}$$

where the non-dimensional parameter, A, used to characterize the system is Atwood number:

$$A = \frac{\rho_s - \rho_g}{\rho_s + \rho_g} \tag{11}$$

and the value of α is between 0.05 and 0.07 (Youngs, 1984; Linden et al., 1994; Snider and Andrews, 1996).

A rectangular domain (0.1 m X 0.6 m X 0.1 m) is chosen for simulating this system. The values for fluid and particle properties are borrowed from the work of Snider (2001). A larger value of particle diameter is used and the interphase drag coefficient ($\propto 1/d_p$) is scaled accordingly. The list of parameters used in this exercise are summarized in Table 6.

Table 6: Material Properties used in Rayleigh-Taylor Instability Simulations

	Case 1	Case 2	Case 3
Particle diameter (m)	2×10^{-6}	2×10^{-6}	2×10^{-6}
Particle density (kg/m^3)	3	5	7
Fluid density (kg/m^3)	1	1	1
Fluid viscosity (Pa-s)	0.001	0.001	0.001
Atwood number	0.1667	0.2857	0.4737
Drag coefficient, $\boldsymbol{\beta}$ (kg m^{-3} s^{-1})	$100\rho_s\varepsilon_s$	$100\rho_s\varepsilon_s$	$100\rho_s\varepsilon_s$

Setup

Computational/Physical Model

3D, transient
Multiphase
Thermal energy equation is not solved

Turbulence equations are not solved (Laminar)
Uniform mesh
First order upwind discretization scheme

Geometry

Coordinate system	Cartesian	Grid Partitions
Channel length, L (x)	0.10 (m)	40
Channel height, H (y)	0.60 (m)	240
Channel width, W (z)	0.10 (m)	40

Material

Gas density, ρ_g	1.0 (kg·m^{-3})
Gas viscosity, μ_g	1.8E-5 (Pa·s)

Solids Type	PIC
Diameter	0.001 (mm)
Density	Refer to Table 6 (kg·m^{-3})

Solids Properties (PIC)

Pressure linear scale factor, P_s	1.0 (N m^{-2})
Exponential scale factor, γ	4.0 (-)
Statistical weight	7.2 X 10^8 (-)

Initial Conditions

x-velocity, u_g, u_m	0.0 (m·s^{-1})
y-velocity, v_g, v_m	0.0 (m·s^{-1})
z-velocity, w_g, w_m	0.0 (m·s^{-1})
Gas volume fraction, ε_g	0.80 (-)
Pressure, p_g	101,325 (Pa)

Boundary Conditions

Top boundary	Pressure outflow
All other boundaries	Free-slip wall

Results

The contour plots (Figure 7) show the evolution of volume fraction fields at the end of 1 second. The instability is triggered by a non-homogenous solids concentration field due to inherent randomness in generating the parcels. The instability is more pronounced at higher values of A. Figure 8 shows the time evolution of the mixing layer, where the coordinates used by Snider (2001) are used. The results are consistent with the work of Snider (2001). The analytical value for the slope of this curve based on Equation (10) is $\sqrt{\alpha}$, which is matched reasonably well by MFiX-PIC. As A increases, the particles reach the bottom of the domain sooner resulting in the associate curve reaching a plateau.

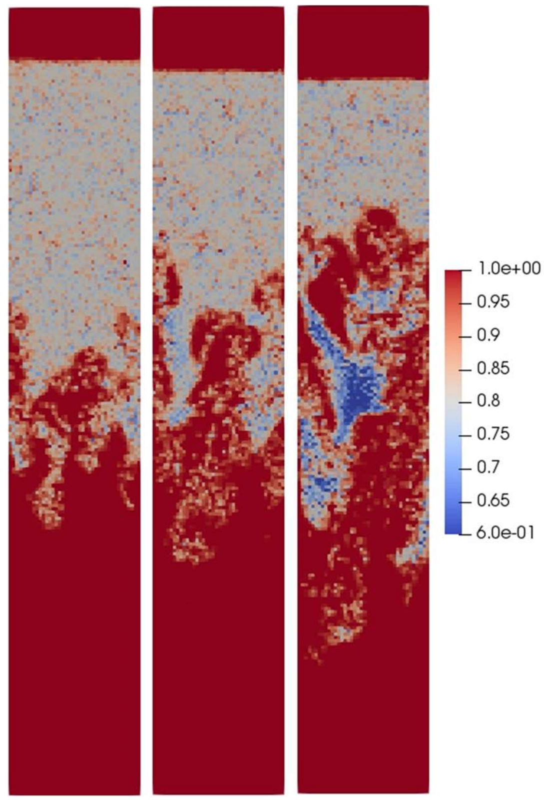

Figure 7: Sectional view of volume fraction contour of the lighter phase at t = 0.8s; A = 0.1667, 0.2857, and 0.4737 (left to right).

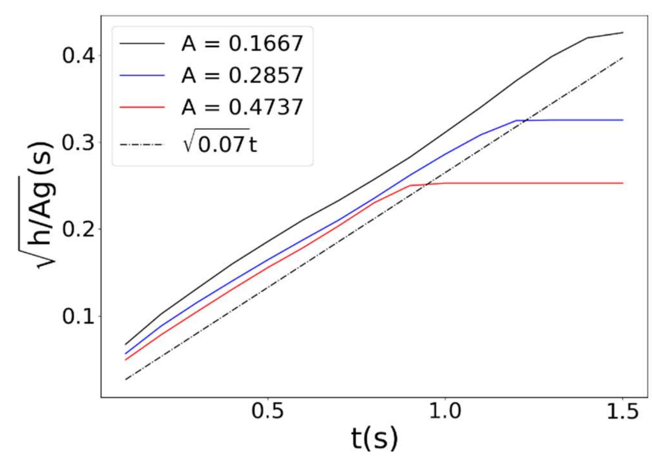

Figure 8: Evolution of mixing layer for A = 0.1667, 0.2857, and 0.4737. The dashed line is the theoretical solution, Equation (28) where α =0.07.

3.2 MINIMUM FLUIDIZATION

Description

A minimum fluidization test is used to validate the interphase momentum transfer between gas and particles. In contrast to particles settling in a quiescent fluid medium described in Section 2.3, a gas phase enters the domain through the bottom boundary, initially through a fixed bed of particles. Once the minimum fluidization condition is reached, the particles change from a fixed state to a fluidized state. This action is accompanied by a change in pressure drop across the bed. The physical experiments were performed at NETL using high-density polyethylene (HDPE) particles in a rectangular domain (0.05 m X 0.20 m X 0.05 m). The mean diameter and density of HDPE are 870 µm and 860 kg/m^3. Figure 9 shows the plot of pressure drop as a function of gas velocity, where the pressure drop is normalized by the weight of bed given by,

$$\Delta P^* = \frac{\Delta P}{mg/A} \tag{12}$$

where ΔP is the pressure drop across the bed, g is the mass of bed material, g is acceleration due to gravity and A is the cross-sectional area of the bed. There is a sharp transition between fixed and fluidized states which marks the minimum fluidization condition. The graphical abscissa at this transition is recognized as the minimum fluidization velocity and the ordinate is the pressure drop that corresponds to the weight of bed material. Based on linear fit between the two regions, minimum fluidization velocity for the case shown is 0.182 m/s.

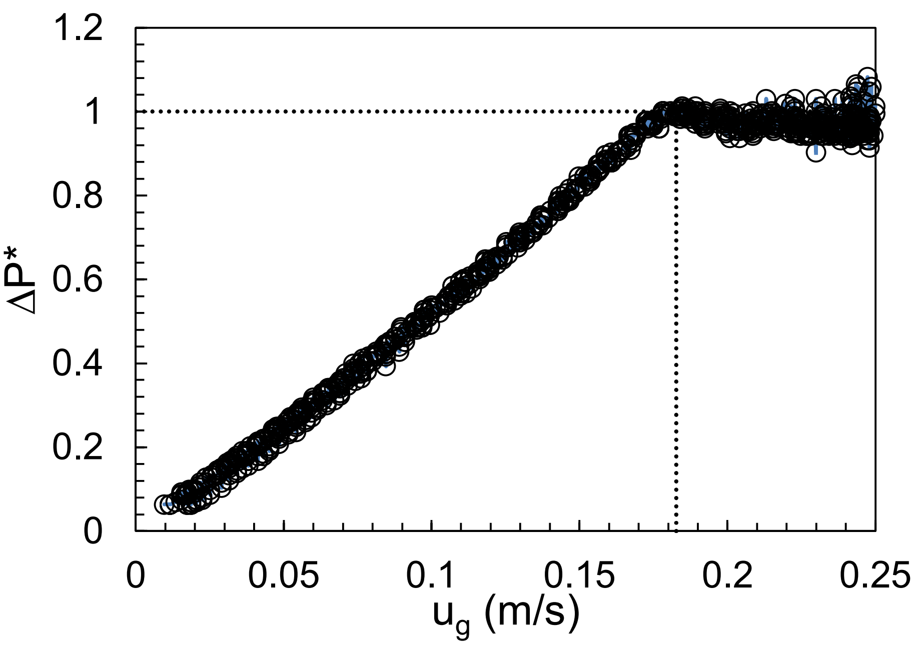

Figure 9: Normalized pressure drop as a function of inlet gas velocity.

Considering the size of particles, it was decided to use a larger domain which could accommodate more computational parcels. Hence, this study used a rectangular domain (0.10 m

X 0.40 m X 0.10 m). The drag correlation of Wen and Yu (1966) is used for calculating the drag coefficient β given by,

$$C_D = \begin{cases} \frac{24}{Re}(1+0.15Re^{0.687}), & Re < 1000 \\ 0.44, & Re > 1000 \end{cases} \tag{13}$$

The particle's Reynolds number is defined as,

$$Re = \frac{\rho_g \varepsilon_g |u_g - u_s| d_p}{\mu_g} \tag{14}$$

where, ρ_g, ε_g, u_g, and μ_g represent density, volume fraction, velocity, and dynamic viscosity of the gas phase. u_s and d_p are the velocity and diameter of particles in the solids phase (Note: d_p is the diameter of particle and not particle).

Setup

Computational/Physical Model

3D, Transient
Multiphase
Thermal energy equation is not solved
Turbulence equations are not solved (Laminar)
Uniform mesh
First order upwind discretization scheme

Geometry

Coordinate system	Cartesian	Grid Partitions
Channel length, L (x)	0.10 (m)	10
Channel height, H (y)	0.40 (m)	40
Channel width, W (z)	0.10 (m)	10

Material

Gas density, ρ_g	1.0 (kg·m^{-3})
Gas viscosity, μ_g	1.8E-5 (Pa·s)
Solids Type	PIC
Diameter	0.87 (mm)
Density	860 (kg·m^{-3})

Solids Properties (PIC)

Pressure linear scale factor, P_s	10.0 (N m^{-2})
Exponential scale factor, γ	3.0 (-)
Statistical weight	4, 5, 10 (-)

Gas volume fraction at packing, ε^*	0.44 (-)	
Initial Conditions		
x-velocity, u_g, u_m	0.0 ($m \cdot s^{-1}$)	
y-velocity, v_g, v_m	0.0 ($m \cdot s^{-1}$)	
z-velocity, w_g, w_m	0.0 ($m \cdot s^{-1}$)	
Gas volume fraction, ε_g	0.82 (-)	
Pressure, p_g	101,325 (Pa)	
Boundary Conditions		
Mass inflow, u_g	Varied ($m\ s^{-1}$)	
Pressure outflow	101,325 (Pa)	Free-slip wall
West, east, north and south boundaries		No-slip wall

Results

Time-dependent boundary velocity for the gas-phase is specified through a user-defined subroutine. A linear ramp function is used, and pressure drop across the bed is extracted at regular intervals. It is worth reiterating that the domain considered for this numerical exercise is different from physical experiments, hence this study does not to show the experimental curve in the resulting plots. However, minimum fluidization is expected to be the same barring minor differences due to factors including wall effects. The transition between fixed and fluidized states is not distinctly predicted by MFiX-PIC (Figure 10) as observed in the experiments. MFiX-PIC does not reproduce the behavior of HDPE particles at minimum fluidization velocity. This could be due to the nature of the particle-stress closure or uncertainty in model parameters. This could also point to a limitation of MFiX-PIC in modeling the fluidization transition from a fixed bed state. However, PIC is capable of predicting the pressure drop corresponding to the weight of bed material, further away from minimum fluidization conditions.

Figure 10 also highlights the negligible effect of parcel size for this case. Sensitivity of ε^* and P_s are also analyzed. For the range of P_s considered in this study, the behavior is unchanged for all practical purposes as observed in Figure 11. However, as ε^* changed there is a noticeable difference in the fluidization behavior (Figure 12). Maximum sensitivity was observed for ε^* among other parameters considered in this study. A more systematic approach is required to draw further conclusions on the observed behavior.

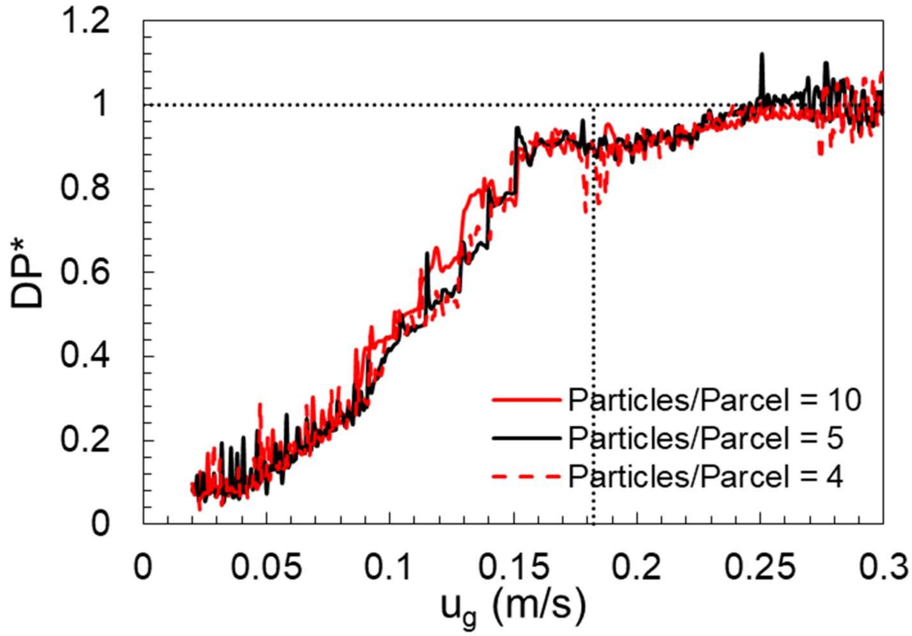

Figure 10: Effect of statistical weight (particles per parcel) on fluidization curve using MFiX-PIC.

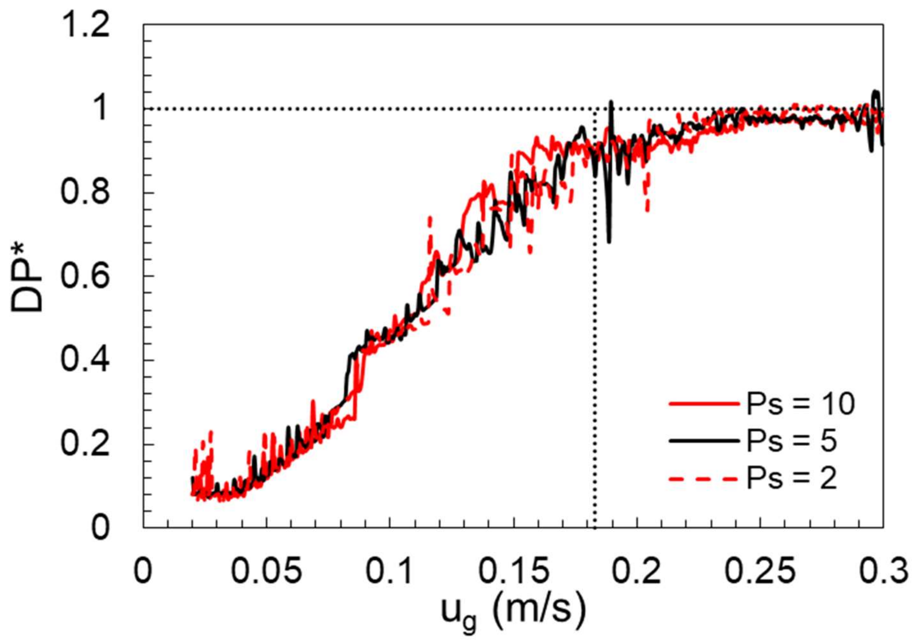

Figure 11: Effect of varying P_s.

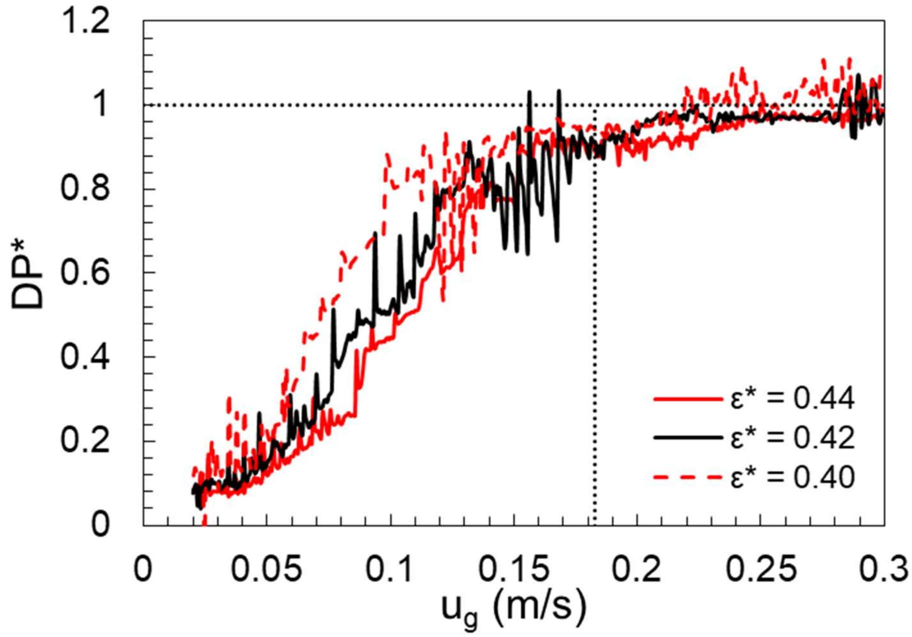

Figure 12: Effect of varying volume fraction at packing.

3.3 CIRCULATING FLUIDIZED BED

Description

Lab-scale circulating fluidized bed experiments were conducted by Xu et al. (2017) to analyze the multi-phase hydrodynamics at multiple flow rates. The schematic of the setup along with the geometry used for computations is shown in Figure 13. Several pressure ports were used to measure pressure drop across different geometric sections. Standpipe height was measured using a high-speed camera and the open-source software, ImageJ, was used for post-processing. The air flow rates were varied at three injection sites using flow controllers FTC180, FTC135, and FTC115 as summarized in Table 7. Please note, the flow rates are measured in Standard Liter per minute (SLPM). The readers are referred to Xu et al. (2017) for further details regarding the physical experiments.

Table 7: Operating Conditions used in Circulating Fluidized Experiments

Operating Condition	FTC180 (SLPM)	FTC135 (SLPM)	FTC115 (SLPM)
Case 1	275	6	1.5
Case 2	300	7.5	2.5
Case 3	325	6	1.5

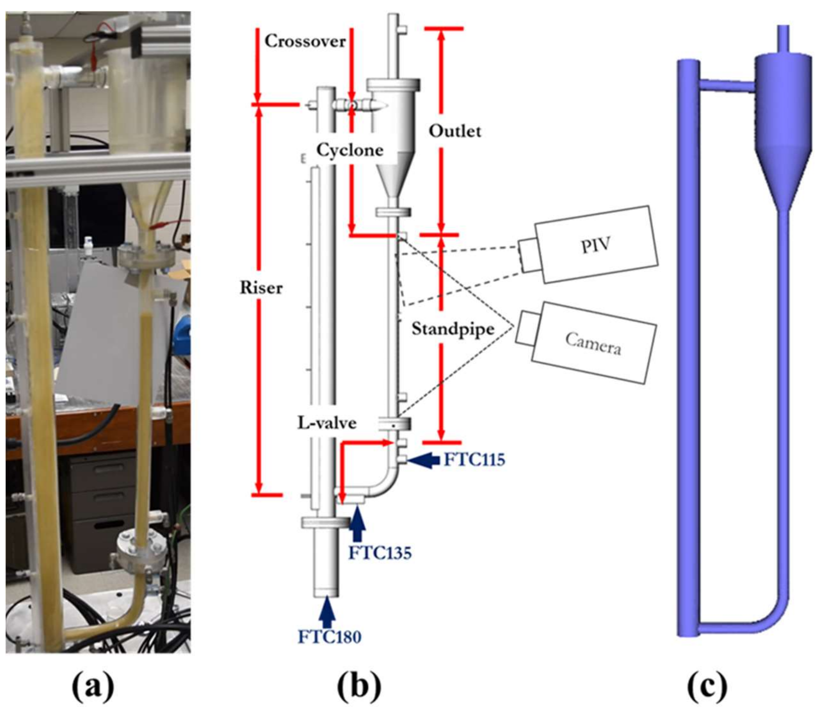

Figure 13: Circulating fluidized bed experiments and computational set-up: (a) snapshot of the experimental facility, (b) schematic of the experimental set-up, and (c) geometry used for simulations.

Setup

Computational/Physical Model

3D, transient
Multiphase
Thermal energy equation is not solved
Turbulence equations are not solved (Laminar)
Uniform mesh
First order upwind discretization scheme

Geometry

Coordinate system	Cartesian	Grid Partitions
Length, L (x)	0.32 (m)	40
Height, H (y)	1.32 (m)	165
Width, W (z)	0.15 (m)	19

Material

Gas density, ρ_g	1.28 (kg·m^{-3})
Gas viscosity, μ_g	1.8E-5 (Pa·s)
Solids Type	PIC
Diameter	0.87 (mm)
Density	860 (kg·m^{-3})

Solids Properties (PIC)

Pressure linear scale factor, P_s	100.0 (N m^{-2})
Exponential scale factor, γ	3.0 (-)
Statistical weight	4 (-)
Solids slip velocity scale factor	0.98 (-)

Initial Conditions

x-velocity, u_g, u_m	0.0 (m·s^{-1})
y-velocity, v_g, v_m	0.0 (m·s^{-1})
z-velocity, w_g, w_m	0.0 (m·s^{-1})
Gas volume fraction in standpipe, ε_g	0.40 (-)
Pressure, p_g	101,325 (Pa)

Boundary Conditions

Mass inflow, u_g	Varied (Table 7) (m s^{-1})	
Pressure outflow	101,325 (Pa)	
All other STL boundaries		No-slip walls

Results

MFiX-PIC simulations are performed using the flow rates listed in Table 7. The drag model of Hill et al. (2001) was used which was found to predict the pressure drop and the standpipe height reasonably well for MFiX-DEM simulations (Xu et al., 2017). Instantaneous contour plots of gas volume fraction are shown in Figure 14 to visualize the solids inventory under different operating conditions. Table 8 summarizes the pressure drop values across the riser and standpipe. The results are also compared with the measurements from experiments along with MFiX-DEM predictions of Xu et al. (2017). There is evidently a trade-off between speed and accuracy between MFiX-DEM and MFiX-PIC. While MFiX-DEM is more accurate since individual trajectories of particles are resolved, MFiX-PIC is up to 8 times faster for the lab-scale circulating fluidized bed experiments while comparing the wall clock time on the same number of cores. This could be attributed to the fact that the particle collisions are modeled using an empirical closure for particle stress. In addition to the pressure drop measurements, the height of inventory in standpipe is also compared. For Cases 1 and 2, the height seems to be over-predicted while it is under-predicted for Case 3. Overall, the results obtained using MFiX-PIC are promising. Further analysis is required to ensure consistency in MFiX-PIC predictions.

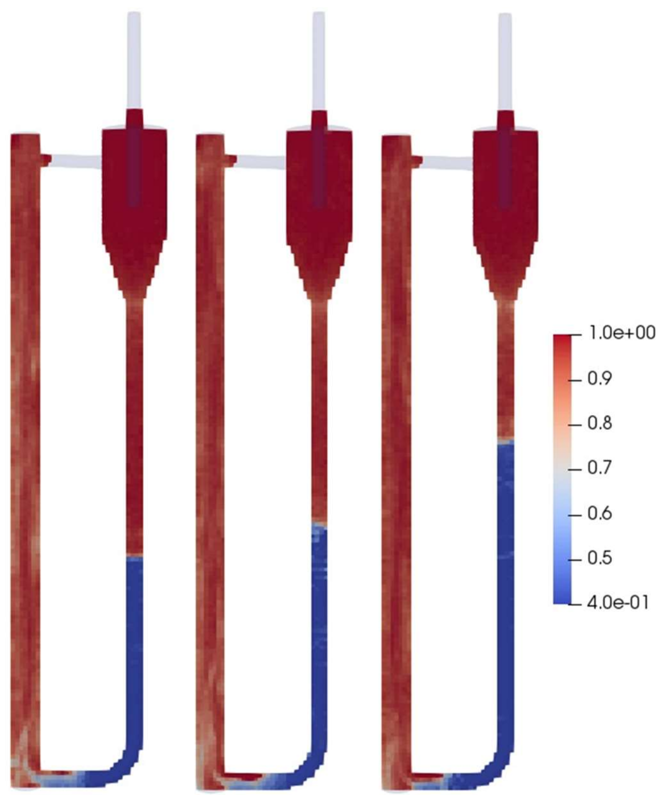

Figure 14: Cross-sectional view (Z-normal) of gas volume fraction contours at t = 20 seconds for Case 1, 2 and 3 (left to right).

Table 8: Comparison of Pressure Drop across Riser and Standpipe

	Pressure Drop across Riser (Pa)			Pressure Drop across Standpipe (Pa)		
	Experiment	MFiX-PIC	MFiX-DEM	Experiment	MFiX-PIC	MFiX-DEM
Case 1	857.00	837.69	973.39	843.23	818.64	802.58
Case 2	816.08	769.03	835.63	1021.25	1050.35	1014.05
Case 3	553.81	643.35	616.98	881.18	1010.24	896.06

Table 9: Height of the Inventory in Standpipe

	Experiment	MFiX-PIC	MFiX-DEM
Case 1	0.43±0.01	0.482	0.42
Case 2	0.47±0.01	0.518	0.50
Case 3	0.65±0.01	0.609	0.68

4. CONCLUSIONS AND FUTURE WORK

An extensive plan for verification and validation of MFiX-PIC has been adopted. The focus of work presented in this report was on systems containing a single solids-phase with mono-dispersed particles. The cases range from unit tests to a lab-scale circulating fluidized bed, and showcase the applicability of PIC for modeling hydrodynamics, as well as heat and mass transfer. An optimal set of model parameters have been employed and reasonable results were obtained. The following are some of the major conclusions from this study:

1. For particle settling and Rayleigh-Taylor instability, $P_s = 1$ was found to yield reasonable predictions while for the circulating fluidized bed, the value had to be increased to $P_s = 100$. This could be due to increased stress in the solids-phase due to impact at higher velocities.
2. A unit test (evaporation) was used to verify the implementation of routines linked to heat and mass transfer. All other tests were pertaining to the verification and validation of hydrodynamics.
3. The minimum fluidization test case could be considered an exception since the transition behavior was not captured accurately by MFiX-PIC. This could be due to an inherent limitation in PIC methodology to account for stress in particles when they transition from being packed to unpacked. This could also point to uncertainty in model parameters.
4. The computational efficiency of MFiX-PIC was noticeable for the circulating fluidized bed setup, where the MFiX-DEM approach was found to have a considerably slower turnaround time. The example highlighted the trade-off between speed and resolution, where the maximum error in pressure drop calculations with MFiX-PIC was found to be close to 16%.
5. Based on our experience so far, reasonable results have been obtained when a single parcel volume is no more than 5% of grid volume. This upper bound on parcel size is expected to yield a physically consistent stress field in the solids-phase.

The study highlights the applicability of PIC methodology for large-scale industrial applications where the particle count becomes intractable for DEM approach. Also, it is observed that for the validation cases considered in this study, the model uncertainty associated with PIC can be reasonably bounded making PIC all the more a viable option. Future plans include performing a rigorous parametric study for some of the conditions covered in this study, and, if possible, establishing sensitivities of PIC parameters to the different response variables. The roadmap proposed by Gel et al. (2018) could be used as a guideline for designing experiments and/or a simulation campaign. From a development perspective, it is of interest to look at alternatives for modeling dilute and dense regimes simultaneously using a blended acceleration approach similar to the work of O'Rourke and Snider (2014). Also, effects informed by polydispersity would be considered in the future that would aim at capturing correct segregation behavior. Further advancement of V&V for PIC largely depends on reliable datasets from large-scale experiments. The inherent assumptions in PIC methodology would make it more suitable for systems having significant particle count (probably of the order of millions or billions) whereby computational parcels have appreciable statistical weight. Objectively assessed data with measurement uncertainties meeting such requirements are scarce in literature. This necessitates a dedicated exercise to generate high-quality reliable datasets which could be used for benchmarking PIC methodology.

5. REFERENCES

AIAA. *AIAA Guide for the Verification and Validation of Computational Fluid Dynamics Simulations*; American Institute of Aeronautics and Astronautics, 1998.

Allen, T. US Department of Defense modeling and simulation: new approaches and initiatives. *Information and Security: An International Journal* **2009,** *23*, 32–48.

Andrews, M. J.; O'Rourke, P. J. The multiphase particle-in-cell (MP-PIC) method for dense particle flow. *International Journal of Multiphase Flow* **1996,** *22*, 379–402.

Auzerais, F.; Jackson, R.; Russel, W. The resolution of shocks and the effects of compressible sediments in transient settling. *Journal of Fluid Mechanics* **1988,** *195*, 437–462.

Bakshi, A.; Shahnam, M.; Gel, A.; Li, T.; Altantzis, C.; Rogers, W.; Ghoneim, A. F. Comprehensive multivariate sensitivity analysis of CFD-DEM simulations: Critical model parameters and their impact on fluidization hydrodynamics. *Powder Technology* **2018,** *338*, 519–537.

Committee, A. P. *Standard for Verification and Validation in Computational Fluid Dynamics and Heat Transfer*; American Society of Mechanical Engineers, 2009.

Garg, R.; Galvin, J.; Li, T.; Pannala, S. Documentation of open-source MFIX-DEM software for gas-solids flows; February 1, 2010. https://mfix.netl.doe.gov/doc/mfix-archive/mfix_current_documentation/dem_doc_2012-1.pdf (accessed August 15, 2019).

Gel, A.; Shahnam, M.; Subramniyan, A. K. Quantifying uncertainty of a reacting multiphase flow in a bench-scale fluidized bed gasifier: A Bayesian approach. *Powder Technology* **2017,** *311*, 484–495.

Gel, A.; Shahnam, M.; Musser, J.; Subramaniyan, A. K.; Dietiker, J. -F. Nonintrusive uncertainty quantification of computational fluid dynamics simulations of a bench-scale fluidized-bed gasifier. *Industrial & Engineering Chemistry Research* **2016,** *55*, 12477–12490.

Gel, A.; Vaidheeswaran, A.; Musser, J.; Tong, C. Toward the Development of a Verification, Validation, and Uncertainty Quantification Framework for Granular and Multiphase Flows—Part 1: Screening Study and Sensitivity Analysis. *Journal of Verification, Validation and Uncertainty Quantification* **2018,** *3*, 031001.

Hill, R.; Koch, D.; Ladd, A. The first effects of fluid inertia on flows in ordered and random arrays of spheres. *Journal of Fluid Mechanics* **2001,** *448*, 213–241.

Linden, P. F.; Redondo, J. M.; Youngs, D. L. Molecular Mixing in Rayleigh–Taylor Instability. *Journal of Fluid Mechanics* **1994,** *265*, 97–124.

Mills, A. F. *Basic Heat and Mass Transfer*; Prentice Hall, Upper Saddle River, 1999.

Musser, J.; Vaidheeswaran, A.; Clarke, M. A. *MFIX Documentation Volume 3: Verification and Validation Manual*; NETL Technical Report Series; Morgantown, WV, 2018.

O'Rourke, P. J.; Snider, D. Inclusion of collisional return-to-isotropy in the MP-PIC method. *Chemical Engineering Science* **2012,** *80*, 39–54.

O'Rourke, P. J.; Snider, D. A new blended acceleration model for the particle contact forces induced by an interstitial fluid in dense particle/fluid flows. *Powder Technology* **2014,** *256*, 39–51.

O'Rourke, P. J.; Zhao, P.; Snider, D. A model for collisional exchange in gas/liquid/solid fluidized beds. *Chemical Engineering Science* **2009,** *64*, 1784–1797.

Shahnam, M.; Gel, A.; Dietiker, J. -F.; Subramaniyan, A. K.; Musser, J. The effect of grid resolution and reaction models in simulation of a fluidized bed gasifier through nonintrusive uncertainty quantification techniques. *Journal of Verification, Validation and Uncertainty Quantification* **2016,** *1*, 041004.

Snider, D. M. An Incompressible Three-Dimensional Multiphase Particle-in-Cell Model for Dense Particle Flows. *Journal of Computational Physics* **2001,** *170*, 523–549.

Snider, D. M.; Andrews, M. J. The structure of shear driven mixing with an unstable thermal stratification. *Journal of Fluids Engineering* **1996,** *118*, 55–60.

Steele, M. J. *Standard for Models and Simulations*; NASA, 2016.

Wallis, G. B. *One Dimensional Two-Phase Flow*; McGraw-Hill: New York, 1969.

Wen, C. Y.; Yu, Y. H. Mechanics of Fluidization. *Chemical Engineering Progress Symposium Series* **1966,** *62*, 100–111.

Xu, Y.; Musser, J.; Li, T.; Gopalan, B.; Panday, R.; Tucker, J.; . . . Rogers, W. A. Numerical Simulation and Experimental Study of the Gas–Solid Flow Behavior Inside a Full-Loop Circulating Fluidized Bed: Evaluation of Different Drag Models. *Industrial and Engineering Chemistry Research* **2017,** *57*, 740–750.

Youngs, D. L. Numerical simulation of turbulent mixing by Rayleigh-Taylor instability. *Physica D: Nonlinear Phenomena* **1984,** *12*, 32–44.

APPENDIX

An analytical expression can be obtained for the velocity of kinematic shocks (also referred to as concentration shocks). Two shock fronts develop in a settling system as depicted in Figure 15. One of the shocks propagates in the direction of gravity (downward), while the other is aligned with the direction of packing (upward).

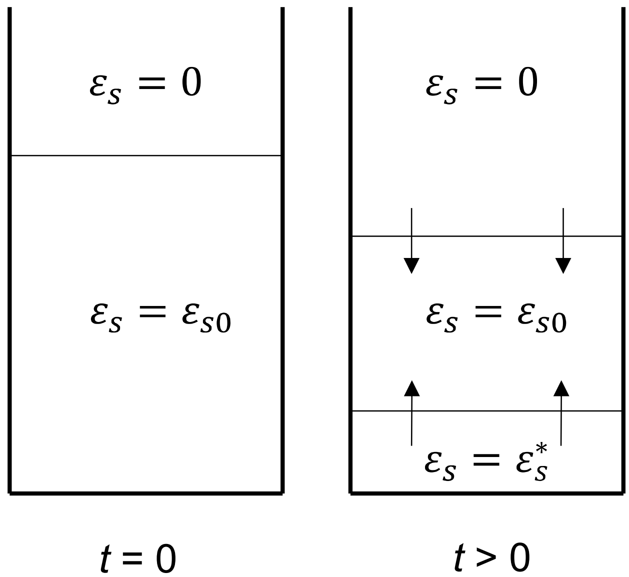

Figure 15: Schematic showing the settling problem.

Settling is governed by the balance between drag, gravity, and buoyancy. Consider the two-fluid model (TFM) system of equations. The phasic continuity equations are given by,

$$\frac{\partial}{\partial t}\rho_g\varepsilon_g + \frac{\partial}{\partial x_j}\left(\rho_g\varepsilon_g u_{gj}\right) = R_g \tag{15}$$

$$\frac{\partial}{\partial t}\rho_s\varepsilon_s + \frac{\partial}{\partial x_j}\left(\rho_s\varepsilon_s u_{sj}\right) = R_s \tag{16}$$

where ρ_g, ε_g, u_{gj}, and R_g represent density, volume fraction, j^{th} component of velocity, and mass source term of the gas phase respectively. The corresponding terms in the solid phase continuity equations are represented with the subscript "s". The phasic momentum equations are given by,

$$\frac{\partial}{\partial t}\rho_g\varepsilon_g u_{gi} + \frac{\partial}{\partial x_j}\left(\rho_g\varepsilon_g u_{gi}u_{gj}\right)$$
$$= -\varepsilon_g\frac{\partial P_g}{\partial x_i} + \frac{\partial}{\partial x_j}\left(\varepsilon_g\tau_{gij}\right) + \beta\left(u_{si} - u_{gi}\right) + \rho_g\varepsilon_g g_i + S_{gi} \tag{17}$$

$$\frac{\partial}{\partial t}\rho_s\varepsilon_s u_{si} + \frac{\partial}{\partial x_j}\left(\rho_s\varepsilon_s u_{si}u_{sj}\right)$$
$$= -\varepsilon_s\frac{\partial P_g}{\partial x_i} + \frac{\partial}{\partial x_j}\left(\varepsilon_s\tau_{sij}\right) + \beta\left(u_{gi} - u_{si}\right) + \rho_s\varepsilon_s g_i + S_{si} \tag{18}$$

P_g, τ_g, S_{gi} represent the pressure, shear stress, and source term in the gas phase. τ_{sij} contains contributions from inter-particle collisions, and S_{si} represents the momentum source term in the solids phase. The following assumptions are made for the settling problem:

1. One-dimensional
2. Shear-stress terms are negligible
3. Particle-particle and particle-wall interactions are negligible
4. Isothermal with no phase change
5. Both the phases are incompressible

Based on these assumptions, the continuity Equations (15), (16) can be combined to give,

$$\frac{\partial}{\partial x}\left(\varepsilon_g u_g\right) + \frac{\partial}{\partial x}\left(\varepsilon_s u_s\right) = \frac{dj}{dx} = 0 \tag{19}$$

The notation for velocity components is dropped since one-dimensional analysis is used. It is seen that the volumetric flux j is a constant for the problem considered. The momentum equations can be simplified to give,

$$-\frac{\partial P_g}{\partial x_i} + \frac{\beta}{\varepsilon_g}u_r + \rho_g g = 0, \tag{20}$$

$$-\frac{\partial P_g}{\partial x_i} - \frac{\beta}{\varepsilon_s}u_r + \rho_s g = 0 \tag{21}$$

where, $u_r = u_s - u_g$ is the relative velocity. Subtracting Equation (21) from Equation (20) gives a relation between the relative velocity, drag function β and gravity as follows,

$$u_r = \frac{g\Delta\rho}{\beta}\varepsilon_g\varepsilon_s \tag{22}$$

where, $\Delta\rho = \rho_s - \rho_g$. The drag function β is given by,

$$\beta = \frac{3}{4}\frac{\rho_g\varepsilon_g\varepsilon_s C_D u_r}{d_p}\varepsilon_g^{-2.65} \tag{23}$$

The drag coefficient for Stokes' law follows,

$$C_D = \frac{24}{Re} = \frac{24\mu_g}{\rho_g u_r d_p \varepsilon_g} \tag{24}$$

The final expression for relative velocity considering Stokes' drag law is given by,

$$u_r = \frac{g\Delta\rho d_p^2}{18\mu_g}\varepsilon_g^{3.65} \tag{25}$$

The laboratory and traveling frame of references are depicted in Figure 16. The quantities are related as follows:

$$\begin{aligned} u'_{gA} &= u_{gA} + u_{shock}, \\ u'_{gB} &= u_{gB} + u_{shoc}\ , \\ u'_{sA} &= u_{sA} + u_{shock}, \\ u'_{sB} &= u_{sB} + u_{shock} \end{aligned} \tag{26}$$

The variables with $'$ denote the traveling frame of reference. The phasic volumetric fluxes are related by,

$$\begin{aligned} j'_{gA} &= j_{gA} + \varepsilon_{gA}u_{shock}, \\ j'_{gB} &= j_{gB} + \varepsilon_{gB}u_{shock}, \\ j'_{sA} &= j_{sA} + \varepsilon_{sA}u_{shock}, \\ j'_{sB} &= j_{sB} + \varepsilon_{sB}u_{shock} \end{aligned} \tag{27}$$

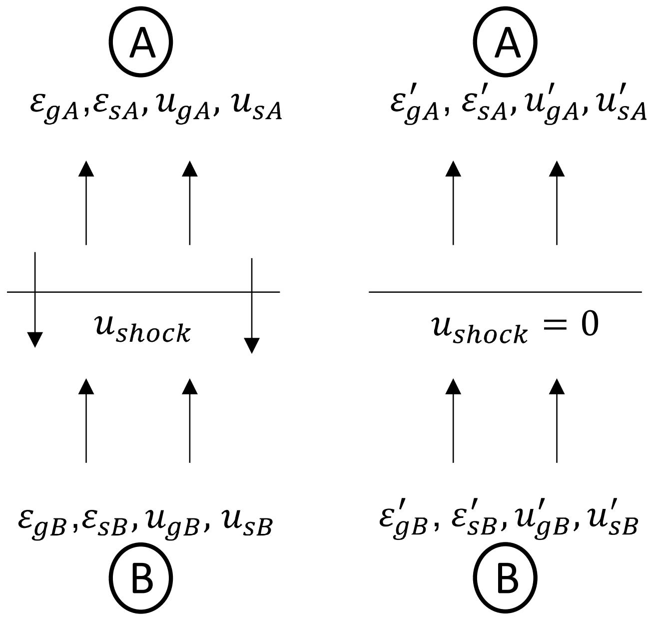

Figure 16: Laboratory (left) and traveling (right) frame of references for the kinematic shock wave.

Since there is no exchange of mass before and after the kinematic shock, additional constraints are obtained as follows,

$$\begin{aligned} j'_{gA} &= j'_{gB}, \\ j'_{sA} &= j'_{sB} \end{aligned} \tag{28}$$

Simplifying Equations (26), (27) and (28), the shock velocity is obtained as,

$$u_{shock} = -\frac{j_{sB} - j_{sA}}{\varepsilon_{sB} - \varepsilon_{sA}} \tag{29}$$

The phasic volumetric flux j_s is related to the total volumetric flux and drift flux (Wallis, 1969) as follows,

$$j_s = \varepsilon_s j + j_{gs}, \tag{30}$$

where, the drift flux j_{gs} is related to the relative velocity as given by Wallis (1969),

$$j_{gs} = \varepsilon_s (u_s - j) = \varepsilon_s \varepsilon_g u_r \tag{31}$$

Upon further simplification of Equation (29) using Equations (30), (31), the analytical expression for shock velocity is obtained as follows,

$$u_{shock} = -\left(j + \frac{\left(\varepsilon_s \varepsilon_g u_r\right)_B - \left(\varepsilon_s \varepsilon_g u_r\right)_A}{\varepsilon_{sB} - \varepsilon_{sA}}\right) \tag{32}$$

where, the relative velocity u_r is given by Equation (25).

This page intentionally left blank.

Brian Anderson, Ph.D.
Director
National Energy Technology Laboratory
U.S. Department of Energy

John Wimer
Associate Director
Strategic Planning
Science & Technology Strategic Plans
& Programs
National Energy Technology Laboratory
U.S. Department of Energy

Bryan Morreale
Executive Director
Research & Innovation Center
National Energy Technology Laboratory
U.S. Department of Energy

NETL Technical Report Series